Available online at www.sciencedirect.com
ScienceDirect
Journal of Computational Physics 224 (2007) 389–402
JOURNAL OF COMPUTATIONAL PHYSICS
www.elsevier.com/locate/jcp

A modal-based multiscale method for large eddy simulation

E.A. Munts *, S.J. Hulshoff, R. de Borst

Faculty of Aerospace Engineering, Delft University of Technology, P.O. Box 5058, 2600 GB, Delft, The Netherlands

Received 1 September 2006; received in revised form 5 March 2007; accepted 6 March 2007
Available online 16 March 2007

Abstract

We introduce a modal spectral element method which employs the variational multiscale approach for large eddy simulation. The method is sufficiently general for application to complex flow geometries, but requires relatively few degrees of freedom for a given mesh and polynomial order. We investigate the performance of the method for fully-developed turbulent channel flow. It is shown that large increases in accuracy can be obtained when the basic dynamics of near-wall coherent structures can be represented using the portion of the modal basis which is free of the subgrid-scale model. This implies that in spite of its lack of orthogonality, the modal basis provides sufficient scale separation to exploit the advantages of the variational multiscale approach.

Keywords: Variational multiscale method; Turbulence simulation; Large eddy simulation; Finite element method

1. Introduction

The variational multiscale (VMS) method was introduced by Hughes et al. [7,8,10] as a general framework for deriving models and numerical methods for the simulation of multiscale phenomena present in many engineering problems. These multiscale concepts were extended to turbulence simulation, leading to the development of the VMS method for Large Eddy Simulation (LES) [11]. In the VMS method, the equations of motion for the resolved scales are obtained by 'a priori' scale decomposition and variational projection. When a hierarchical basis is employed to represent the resolved scales of motion, the resulting variational form can be written as a coupled set of equations describing the dynamics of the large resolved and small resolved scales. As described by Collis [1], this leads to the key feature of the VMS approach as it allows for different modeling assumptions for each range of the resolved scales. One typically confines modeling to the equations describing the small resolved scales. In doing so, numerical consistency is retained in the large resolved scales, allowing full rate of convergence of the numerical method used to solve the large-scale equations. When using eddy-viscosity SGS models (as commonly done in LES), this is advantageous compared to traditional LES

* Corresponding author. Tel.: +31 6 55 17 53 40.
E-mail address: e.a.munts@lr.tudelft.nl (E.A. Munts).

0021-9991/$ - see front matter © 2007 Elsevier Inc. All rights reserved.
doi:10.1016/j.jcp.2007.03.004

approaches which suffer from reduced convergence rates in all the resolved scales due to model-related artificial-viscosity effects [9].

Prior VMS implementations have demonstrated promising results for turbulence simulation in simple geometries. The VMS method was first applied to decaying homogeneous isotropic turbulence [12] and turbulent channel flows [13,20] using a global spectral discretization in the homogeneous directions. With a constant-coefficient Smagorinsky model [28] only in the small-scale equation, the VMS method outperformed traditional LES formulations using more complex dynamic models. A finite-element based VMS-LES method employing a hierarchical serendipity-like basis was introduced by Jansen and Tejada-Martínez [14], who applied it to decaying isotropic turbulence. A very general finite-element based approach was also introduced by Collis [2], who merged the VMS method with a high-order accurate discontinuous Galerkin method using an orthogonal basis. An extensive investigation of this VMS discretization in the context of turbulent channel flow was performed by Srinivasan and Collis [23,25]. It was demonstrated that the VMS approach leads to increased computational efficiency compared to traditional LES methods using similar subgrid-scale (SGS) models on all scales. The partition between the large and small scales in a simulation was found to be a crucial parameter for obtaining high-quality solutions. In particular, this partition should be chosen such that the large-scale coherent structures are free from the direct influence of the SGS model. Another VMS formulation capable of handling unstructured domains was introduced by Koobus and Farhat [17], who employed a finite volume/element method, in which scale separation was based on cell agglomeration. Results obtained using this method for a vortex shedding flow past a square cylinder were in better agreement with experimental data than those predicted by a traditional LES formulation.

The application of global spectral methods to the channel problem normally exploits the presence of periodic homogenous planes. This approach can be difficult to extend to more complex flow geometries. Discontinuous Galerkin methods, on the other hand, are very general, but have a relatively large number of degrees of freedom for a given mesh and polynomial order of the solution approximation. A third possibility is to use space-continuous spectral-element methods, which have less degrees of freedom than discontinuous methods for a given mesh and polynomial order. In this paper, we introduce a modal-based space-continuous FEM for VMS-LES. Like the bases used by Hughes and Collis, it is hierarchical in nature, but unlike them it is only approximately orthogonal. We therefore, investigate whether the previously observed advantages of the VMS formulation are realized by the proposed modal-based formulation. To do so we consider its performance for fully-developed turbulent channel flow. We focus on the effect of SGS modeling together with spatial resolution requirements, which leads to guidelines for obtaining reasonable low-order turbulence statistics. In this process, we compare results obtained using the present VMS formulation to those obtained from a traditional LES formulation as well as results obtained using no SGS model.

2. Governing equations

We consider the compressible Navier–Stokes equations in conservation form

$$\mathbf{U}_{,t} + \mathbf{F}_{i,i}(\mathbf{U}) - \mathbf{F}^v_{i,i}(\mathbf{U}) = \mathbf{S}, \tag{1}$$

where $\mathbf{U} = \{\rho, \rho\mathbf{u}, \rho e\}^{\mathrm{T}}$ is the vector of conservative variables, ρ the fluid density, $\mathbf{u} = \{u, v, w\}^{\mathrm{T}}$ the fluid velocity vector, and $e = i + \frac{1}{2}u_i u_i$ the total energy per unit mass, where i the internal energy per unit mass. In the above equations, the Einstein summation convention for repeated indices is employed, and subscripts following a comma denote differentiation with respect to the subscript. The inviscid flux vectors $\mathbf{F}_i(\mathbf{U})$, the viscous flux vectors $\mathbf{F}^v_i(\mathbf{U})$, and the source vector $\mathbf{S}$ are defined as

$$\mathbf{F}_i(\mathbf{U}) = u_i\mathbf{U} + p\begin{Bmatrix} 0 \\ \delta_{1i} \\ \delta_{2i} \\ \delta_{3i} \\ u_i \end{Bmatrix}, \quad \mathbf{F}^v_i(\mathbf{U}) = \begin{Bmatrix} 0 \\ \tau_{1i} \\ \tau_{2i} \\ \tau_{3i} \\ \tau_{ij}u_j - q_i \end{Bmatrix}, \quad \mathbf{S} = \rho\begin{Bmatrix} 0 \\ f_1 \\ f_2 \\ f_3 \\ f_i u_i \end{Bmatrix}, \tag{2}$$

where p is the thermodynamic pressure, δ_{ij} is the Kronecker delta, τ_{ij} is the viscous stress tensor, q_j is the heat flux vector, and f_i is a body force per unit mass. The system of equations (1) is closed by the following constitutive relations

$$\tau_{ij} = 2\mu\left(S_{ij} - \frac{\delta_{ij}}{3}S_{kk}\right), \tag{3}$$

$$q_i = -\kappa T_{,i}, \tag{4}$$

$$p = (\gamma - 1)\rho c_{\mathrm{v}} T, \tag{5}$$

$$i = c_{\mathrm{v}} T, \tag{6}$$

where (3) implies a Newtonian fluid with μ the molecular viscosity coefficient and $S_{ij} = \frac{1}{2}(u_{i,j} + u_{j,i})$ the strain-rate tensor. Eq. (4) is Fourier's law of heat conduction with κ the thermal conductivity coefficient and T the absolute temperature. The equation of state (5) implies a perfect gas (i.e. intermolecular forces are negligible), where $\gamma = c_{\mathrm{p}}/c_{\mathrm{v}}$ with c_{p} and c_{v} the specific heat at constant pressure and constant volume, respectively. Finally, the internal energy is related to the absolute temperature by the caloric equation of state (6).

The Navier–Stokes equations can be written in quasi-linear form

$$\mathbf{U}_{,t} + \mathbf{A}_i \mathbf{U}_{,i} - (\mathbf{K}_{ij}\mathbf{U}_{,j})_{,i} = \mathbf{S}, \tag{7}$$

where $\mathbf{A}_i = \mathbf{F}_{i,\mathbf{U}}$ are the inviscid flux Jacobians and $\mathbf{K}_{ij}$ are the diffusivity matrices, satisfying $\mathbf{K}_{ij}\mathbf{U}_{,j} = \mathbf{F}^v_i$.

The Navier–Stokes equations in conservation form can be solved using any set of variables [6] by introducing a transformation $\mathbf{U} = \mathbf{U}(\mathbf{Y})$, where $\mathbf{Y}$ is a new set of variables. Using this transformation the quasi-linear form (7) can be expressed in terms of $\mathbf{Y}$ as

$$\widetilde{\mathbf{A}}_0 \mathbf{Y}_{,t} + \widetilde{\mathbf{A}}_i \mathbf{Y}_{,i} - (\widetilde{\mathbf{K}}_{ij}\mathbf{Y}_{,j})_{,i} = \mathbf{S}, \tag{8}$$

where

$$\widetilde{\mathbf{A}}_0 = \mathbf{U}_{,\mathbf{Y}}, \quad \widetilde{\mathbf{A}}_i = \mathbf{A}_i \widetilde{\mathbf{A}}_0, \quad \text{and} \quad \widetilde{\mathbf{K}}_{ij} = \mathbf{K}_{ij}\widetilde{\mathbf{A}}_0. \tag{9}$$

For convenience of implementing boundary conditions for channel flow, i.e. no slip and a constant wall temperature, we use $\mathbf{Y} = \{\rho, \mathbf{u}, T\}^{\mathrm{T}}$. The coefficients of $\widetilde{\mathbf{A}}_i$ and $\widetilde{\mathbf{K}}_{ij}$ for the present and alternative sets of variables can be found in refs. [6,19].

3. Finite element discretization

3.1. Space–time topology

The fixed spatial domain for the problem is denoted by Ω, which is an open, bounded subset of $\mathbb{R}^d$, with $d \in \{1,2,3\}$ the spatial dimension, and boundary $\partial\Omega$. Let the time interval of interest $I = (0, T)$ be partitioned into N time slabs $I_n = (t_n, t_{n+1})$. A space–time slab is then defined as $\mathsf{Q}_n = \Omega \times I_n$ with lateral boundary $\mathsf{P}_n = \partial\Omega \times I_n$, as shown in Fig. 1.

Let the spatial domain Ω for the nth space–time slab be subdivided into $(n_{\mathrm{el}})_n$ elements $\Omega^e_n, e = 1, \ldots, (n_{\mathrm{el}})_n$. The space–time elements for the nth slab are then defined as $\mathsf{Q}^e_n = \Omega^e_n \times I_n$.

Within the space–time slabs Q the solution is approximated using polynomials of order P in space and linear in time. Let $\mathscr{P}_k(\widehat{\mathsf{Q}})$ be the space of polynomials of degree $\leqslant P$ defined on the master element $\widehat{\mathsf{Q}} = (-1, 1)^{d+1}$, then

$$\mathscr{P}_P(\mathsf{Q}^e) = \{\phi | \phi = \hat{\phi} \circ \mathscr{T}^{-1}, \hat{\phi} \in \mathscr{P}_k(\widehat{\mathsf{Q}})\}, \tag{10}$$

where $\mathscr{T} : \widehat{\mathsf{Q}} \mapsto \mathscr{T}(\widehat{\mathsf{Q}})$ denotes the mapping from the master element to physical space. The finite element approximation and weighting spaces can then be defined as

$$\mathscr{Y}^h_n = \{\mathbf{Y}^h | \mathbf{Y}^h \in (\mathscr{C}^0(\mathsf{Q}_n))^m, \mathbf{Y}^h|_{\mathsf{Q}^e_n} \in (\mathscr{P}_P(\Omega^e_n) \times \mathscr{P}_1(I_n))^m, \mathbf{Y}^h = \mathbf{g}(t) \quad \text{on } \Gamma_{\mathrm{D}}\}, \tag{11}$$

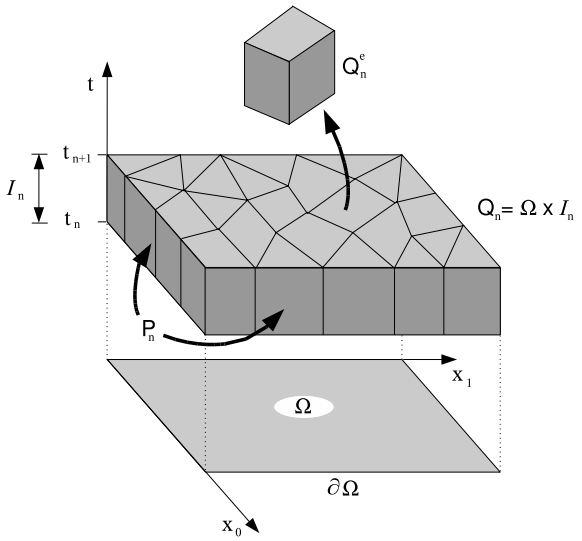

Fig. 1. Sketch of a space–time slab.

and

$$\mathscr{W}_n^h = \{\mathbf{W}^h | \mathbf{W}^h \in (\mathscr{C}^0(\mathsf{Q}_n))^m, \mathbf{W}^h|_{\mathsf{Q}_n^e} \in (\mathscr{P}_P(\Omega_n^e) \times \mathscr{P}_1(I_n))^m, \mathbf{W}^h = \mathbf{0} \quad \text{on } \Gamma_D\}, \tag{12}$$

where $m = d + 2$ is the number of conservative variables, $\mathbf{g}(t)$ is the vector of Dirichlet conditions and Γ_D is the portion of the space–time slab boundary where Dirichlet boundary conditions are specified.

3.2. Time-discontinuous galerkin method

We employ the time-discontinuous Galerkin method [27], so that the variational formulation of the compressible Navier–Stokes equations (1) can then be stated as follows: Within each slab Q_n, find $\mathbf{Y}^h \in \mathscr{Y}_n^h$ such that $\forall \mathbf{W}^h \in \mathscr{W}_n^h$

$$\begin{aligned}
&\int_{\mathsf{Q}_n} (-\mathbf{W}_{,t}^h \cdot \mathbf{U}(\mathbf{Y}^h) - \mathbf{W}_{,i}^h \cdot \mathbf{F}_i(\mathbf{Y}^h) + \mathbf{W}_{,i}^h \cdot \widetilde{\mathbf{K}}_{ij} \mathbf{Y}_{,j}^h) \, \mathrm{d}\mathsf{Q} + \int_{\mathsf{P}_n} \mathbf{W}^h \cdot (\mathbf{F}_i(\mathbf{Y}^h) - \mathbf{F}_i^v(\mathbf{Y}^h)) n_i \, \mathrm{d}\mathsf{P} \\
&\quad + \int_{\Omega} (\mathbf{W}^h(t_{n+1}^-) \cdot \mathbf{U}(\mathbf{Y}^h(t_{n+1}^-)) - \mathbf{W}^h(t_n^+) \cdot \mathbf{U}(\mathbf{Y}^h(t_n^-))) \, \mathrm{d}\Omega \\
&= \int_{\mathsf{Q}_n} \mathbf{W}^h \cdot \mathbf{S} \, \mathrm{d}\mathsf{Q}.
\end{aligned} \tag{13}$$

The third line in (13) is obtained by adding the jump condition

$$\int_{\Omega_n} \mathbf{W}^h(t_n^+) \cdot [[\mathbf{U}(\mathbf{Y}^h(t_n))]] \, \mathrm{d}\Omega \tag{14}$$

to the terms resulting from the integration-by-parts of the time terms. For time-discontinuous Galerkin methods, the jump condition provides the mechanism by which information is propagated from one slab to the next. In other words, it imposes a weakly-enforced boundary condition. When using piecewise-linear basis functions in the temporal direction, this method is third-order accurate in time [27].

To simplify notation, we introduce the following shorthand notation for the variational form (13)

$$B(\mathbf{W}, \mathbf{U}) = (\mathbf{W}, \mathbf{S}). \tag{15}$$

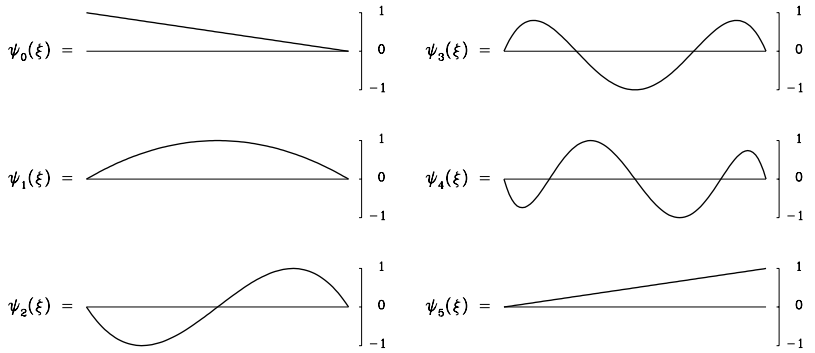

Fig. 2. Shape of the one-dimensional modal expansion for a polynomial degree $P = 5$ and $\alpha = \beta = 1.0$ (From Karniadakis and Sherwin [15], reproduced with permission).

3.3. Spatial finite element basis

Traditionally, finite element methods make use of Lagrangian approximation bases, which consist of a set of (nodal) polynomial basis functions of equal degree. Consequently, these bases do not readily lend themselves to scale decomposition, such as required by the VMS method. Here, we consider a spatially continuous spectral element method, employing a hierarchical high-order polynomial basis [15]. On a one-dimensional master element with $\xi \in (-1, 1)$ this basis is defined as

$$\phi_p(\xi) \mapsto \psi_p(\xi) = \begin{cases} \left(\frac{1-\xi}{2}\right) & p = 0, \\ \left(\frac{1-\xi}{2}\right)\left(\frac{1+\xi}{2}\right) P_{p-1}^{\alpha,\beta}(\xi) & 0 < p < P, \\ \left(\frac{1+\xi}{2}\right) & p = P, \end{cases} \tag{16}$$

where $P_{p-1}^{\alpha,\beta}(\xi)$ are Jacobi polynomials of degree $p - 1$. Although in fact any Jacobi polynomial (e.g. Legendre or Chebychev) can be used, here we employ Jacobi polynomials with $\alpha = \beta = 1.0$ as they are approximately orthogonal, maximizing their suitability for VMS-LES. An example of this basis with $P = 5$ is shown in Fig. 2. For rectangular elements, the multi-dimensional modal bases can be simply constructed by a product of the one-dimensional bases in each of the coordinate directions, as shown in Fig. 3.

Note that the modal basis (16) consists of a hierarchy of polynomials of increasing degree. As the polynomial degree increases, smaller-scale behavior can be captured by the corresponding basis functions. We define the parameter $\widetilde{P}$ to partition the resolved scales into large and small scales, where basis functions of degree $\geqslant \widetilde{P}$ in one or more of the spatial coordinate directions represent the small scales. The large scales are then described by the remaining low order basis functions.

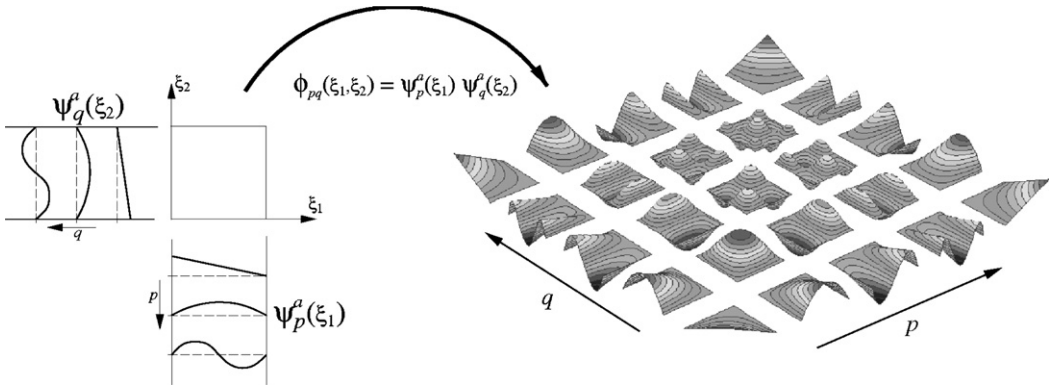

Fig. 3. Construction of a two-dimensional modal expansion basis from the product of two one-dimensional expansions of degree $P_1 = P_2 = 4$ (From Karniadakis and Sherwin [15], reproduced with permission).

4. The variational multiscale method

Here, we give a brief outline of the VMS method. A more detailed description can be found in Collis [1] and Hughes et al. [11]. We follow the three-level multiscale formulation introduced by Collis [1], in which both the solution and weighting functions are decomposed as

$$\mathbf{U} = \overline{\mathbf{U}} + \widetilde{\mathbf{U}} + \widehat{\mathbf{U}}, \qquad \mathbf{W} = \overline{\mathbf{W}} + \widetilde{\mathbf{W}} + \widehat{\mathbf{W}}, \tag{17}$$

where $\overline{\mathbf{U}}$ are the large scales, $\widetilde{\mathbf{U}}$ are the small scales, $\widehat{\mathbf{U}}$ are the unresolved scales, and a similar decomposition is used for the weighting functions. Note that both the large and small scales are part of the resolved scales. The equations describing the dynamics of the large, small and unresolved scales of motion are obtained by substituting (17) into the variational form (15), yielding

$$\begin{aligned}
\text{Large}: &\quad B(\overline{\mathbf{W}}, \overline{\mathbf{U}} + \widetilde{\mathbf{U}} + \widehat{\mathbf{U}}) = (\overline{\mathbf{W}}, \mathbf{S}),\\
\text{Small}: &\quad B(\widetilde{\mathbf{W}}, \overline{\mathbf{U}} + \widetilde{\mathbf{U}} + \widehat{\mathbf{U}}) = (\widetilde{\mathbf{W}}, \mathbf{S}),\\
\text{Unresolved}: &\quad B(\widehat{\mathbf{W}}, \overline{\mathbf{U}} + \widetilde{\mathbf{U}} + \widehat{\mathbf{U}}) = (\widehat{\mathbf{W}}, \mathbf{S}),
\end{aligned}$$

which constitute a coupled set of equations, referred to as the large, small, and unresolved-scale equations. If a non-orthogonal finite element basis is employed, the large-scale equation can be written as

$$B(\overline{\mathbf{W}}, \overline{\mathbf{U}}) + B'(\overline{\mathbf{W}}, \overline{\mathbf{U}}, \widetilde{\mathbf{U}}) - R(\overline{\mathbf{W}}, \widetilde{\mathbf{U}}) = (\overline{\mathbf{W}}, \mathbf{S}) - B'(\overline{\mathbf{W}}, \overline{\mathbf{U}}, \widehat{\mathbf{U}}) + R(\overline{\mathbf{W}}, \widehat{\mathbf{U}}) + C(\overline{\mathbf{W}}, \widetilde{\mathbf{U}}, \widehat{\mathbf{U}}), \tag{18}$$

and the small-scale equation is

$$B'(\widetilde{\mathbf{W}}, \overline{\mathbf{U}}, \widetilde{\mathbf{U}}) - R(\widetilde{\mathbf{W}}, \widetilde{\mathbf{U}}) = -[B(\widetilde{\mathbf{W}}, \overline{\mathbf{U}}) - (\widetilde{\mathbf{W}}, \mathbf{S})] - B'(\widetilde{\mathbf{W}}, \overline{\mathbf{U}}, \widehat{\mathbf{U}}) + R(\widetilde{\mathbf{W}}, \widehat{\mathbf{U}}) + C(\widetilde{\mathbf{W}}, \widetilde{\mathbf{U}}, \widehat{\mathbf{U}}). \tag{19}$$

In these expressions, $B'(\overline{\mathbf{W}}, \overline{\mathbf{U}}, \mathbf{U}')$ is the operator $B(\overline{\mathbf{W}}, \overline{\mathbf{U}})$ linearized about $\overline{\mathbf{U}}$ for a linear perturbation $\mathbf{U}'$, $C(\overline{\mathbf{W}}, \widetilde{\mathbf{U}}, \widehat{\mathbf{U}})$ is the generalized cross-stress projection onto the large scales, and $R(\overline{\mathbf{W}}, \widetilde{\mathbf{U}})$ is the generalized Reynolds-stress projection onto the large scales. The detailed expressions for these terms can be found in Munts [19]. As described by Collis [1], for incompressible flows, $C(\overline{\mathbf{W}}, \widetilde{\mathbf{U}}, \widehat{\mathbf{U}})$ and $R(\overline{\mathbf{W}}, \widetilde{\mathbf{U}})$ are identical to the projection of the cross-stress and Reynolds stress onto the large scales. For compressible flows, these terms are more complicated due to additional terms arising from the variable density and terms in the energy equation.

Next, we make the following SGS modeling assumptions as is typically done in the VMS method [1]. The unresolved scales are assumed to have negligible direct influence on the dynamics of the large scales. Consequently, all terms involving the unresolved scales in the large-scale equation (i.e. the second line in (18)) are set to zero. The small and unresolved scales, on the other hand, are closer in scale and thus the effect of the unresolved scales on the small scales must be modeled. Therefore, all terms involving the unresolved scales in the small-scale equation (i.e. the second line in (19)) are replaced by a model $\mathbf{M}(\widetilde{\mathbf{W}}, \widetilde{\mathbf{U}})$. With these modeling assumptions, the large and small-scale equations become

$$B(\overline{\mathbf{W}}, \overline{\mathbf{U}}) + B'(\overline{\mathbf{W}}, \overline{\mathbf{U}}, \widetilde{\mathbf{U}}) - R(\overline{\mathbf{W}}, \widetilde{\mathbf{U}}) = (\overline{\mathbf{W}}, \mathbf{S}), \tag{20}$$

$$B'(\widetilde{\mathbf{W}}, \overline{\mathbf{U}}, \widetilde{\mathbf{U}}) - R(\widetilde{\mathbf{W}}, \widetilde{\mathbf{U}}) = -[B(\widetilde{\mathbf{W}}, \overline{\mathbf{U}}) - (\widetilde{\mathbf{W}}, \mathbf{S})] + \mathbf{M}(\widetilde{\mathbf{W}}, \widetilde{\mathbf{U}}), \tag{21}$$

respectively. Note that the above modeling assumptions do not imply that the large scales do not feel the influence of the model. In fact, the large scales are still indirectly influenced by the model through its interaction with the small scales. However, the coupling terms in the large-scale equation which provide this interaction are still in their exact form. Moreover, since the large-scale equation does not have explicit modeling terms, it allows full-rate of convergence of the underlying numerical discretization. This key feature is referred to as the consistency property of the large scales with the Navier–Stokes equations [1,11].

A thorough discussion on SGS modeling for compressible flows is provided by Martin et al. [18]. Here, we make the assumption that if the unresolved scales are sufficiently small, their effect can be reasonably modeled using an eddy-viscosity assumption, as is commonly done in LES. This concept stems from the analogy between turbulent stresses and viscous stresses, so that the model term can be written as

$$\mathbf{M}(\widetilde{\mathbf{W}},\widetilde{\mathbf{U}}) = -\int_{\mathsf{Q}_n} \widetilde{\mathbf{W}}_{,i}\cdot\mathbf{F}_i^m(\widetilde{\mathbf{U}})\,\mathrm{d}\mathsf{Q} + \int_{\mathsf{P}_n} \widetilde{\mathbf{W}}\cdot\mathbf{F}_i^m(\widetilde{\mathbf{U}})n_i\,\mathrm{d}\mathsf{P}, \tag{22}$$

where $\mathbf{F}_i^m(\widetilde{\mathbf{U}})$ is the model flux vector

$$\underline{F}_i^m(\widetilde{\mathbf{U}}) = \begin{Bmatrix} 0 \\ \tau_{1i}^m \\ \tau_{2i}^m \\ \tau_{3i}^m \\ \tau_{ij}^m\tilde{u}_j - q_i^m \end{Bmatrix}, \tag{23}$$

with τ_{ij}^m the SGS stress tensor, and q_i^m the SGS heat transfer.

The VMS method employing the constant-coefficient Smagorinsky model [28] has proven to be successful in prior VMS implementations [12–14,22–25]. Therefore, as a first investigation of the present VMS method, this model is also used here. Since the model acts directly on the small scales, the SGS stress tensor is defined as

$$\tau_{ij}^m = 2\mu_t\left(\widetilde{S}_{ij} - \frac{\delta_{ij}}{3}\widetilde{S}_{kk}\right), \quad \mu_t = (C_s\Delta)^2\rho|\widetilde{S}|, \tag{24}$$

where μ_t is the eddy-viscosity coefficient, and $\widetilde{S}_{ij} = \frac{1}{2}(\tilde{u}_{i,j} + \tilde{u}_{j,i})$ is the symmetric part of the small-scale velocity gradient tensor, C_s is the Smagorinsky constant, $|\widetilde{S}| = (2\widetilde{S}_{ij}\widetilde{S}_{ij})^{1/2}$, and Δ is a length scale representative of the unresolved scales, which is computed using

$$\Delta = \left(\frac{\Delta x_1}{P_1}\frac{\Delta x_2}{P_2}\frac{\Delta x_3}{P_3}\right)^{1/3}, \tag{25}$$

where Δx_i represents the element size in the ith direction and P_i is the polynomial degree of the finite-element approximation in the ith direction. Finally, the SGS heat flux in (23) is computed from

$$q_i^m = \kappa_t\frac{\partial\widetilde{T}}{\partial x_i}, \quad \kappa_t = \frac{\mu_t c_p}{Pr_t}, \tag{26}$$

where $Pr_t = 0.9$ is the turbulent Prandtl number [26].

Note that we only consider the small-scale solution components in the SGS model (24), which therefore, corresponds to the so-called small–small variant of the Smagorinsky model [11]. If all the small-scale components in (24) are replaced by all the resolved scales, the classical Smagorinsky model is recovered.

5. Turbulent channel flow

5.1. Problem description

Planar channel flow has been a widely used test case for the research of turbulence in the presence of mean shear. The flow is assumed to be passing between two horizontal plates separated by a distance 2δ as shown in Fig. 4, where $x = x_1$ is the streamwise direction, $y = x_2$ is the wall-normal direction, and $z = x_3$ is the spanwise

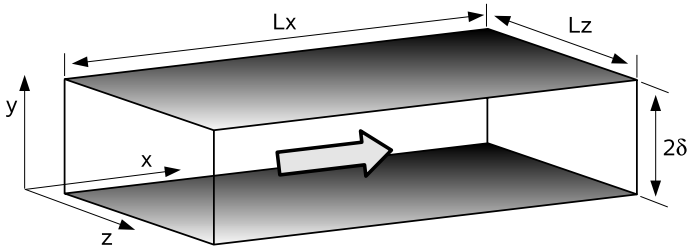

Fig. 4. Planar channel flow geometry. The arrow indicates the direction of the mean flow, and the shaded regions represent the channel walls.

direction. Results for wall bounded turbulent flows are often presented in wall-units, defined as $x_i^+ = x_i u_\tau / \nu$ and $u^+ = u/u_\tau$, where $\nu = \mu/\rho$, and $u_\tau \equiv (\tau_w/\rho)^{1/2}$ is the friction velocity, with τ_w the average wall shear stress.

Numerous experimental and numerical investigations have indicated the presence of regions in the near-wall vicinity of the flow in which the velocity is relatively low compared to their direct surroundings. These near-wall streaks consist of well-defined structures independent of the Reynolds number, having a mean streamwise extent of $\Delta x^+ \approx 400$ and a mean spanwise separation of $\Delta z^+ \approx 100$. Near-wall streaks fall into the category of coherent structures, which play an important role in the dynamics of turbulent flows [21]. It was shown by Collis [3] that the scale partition within the VMS method should be chosen based on the length scales associated with these near-wall streaks. In particular, the basic dynamics of the near-wall streaks should be kept free from the direct influence of the model. It was found that spanwise scale separation lead to sharper estimates of the required partition. This is likely due to the fact that near-wall streaks are more consistently spaced in the spanwise direction. Therefore, when considering near-wall streaks, we focus on the spanwise direction.

5.2. Simulation parameters

We assume the flow to be homogeneous in horizontal planes parallel to the walls, so that periodic boundary conditions can be applied in the streamwise and spanwise directions. As a consequence of the periodic boundary condition in the streamwise direction, the flow cannot be driven by a pressure gradient. Therefore, a constant external body force is applied, which mimics the role of the pressure gradient, i.e. $\mathbf{f} = \{-\mathrm{d}p/\mathrm{d}x, 0, 0\}^{\mathrm{T}}$.

The resolution in the vicinity of the wall is increased by using a stretched mesh in the wall-normal direction [23], such that

$$y_j = \frac{\tanh(a_s(2j/N_y - 1))}{\tanh(a_s)} + 1, \quad j = 0, \ldots, N_y, \tag{27}$$

where N_y is the number of elements in the wall-normal direction and a_s is a stretching factor, which is set equal to $a_s = 1.75$.

At the solid walls we apply the no-slip condition for the velocity components and a constant wall temperature. The latter allows internal energy created by viscous dissipation to be removed from the domain via heat transfer so that a statistically steady state can be achieved.

In the present simulations, we choose the channel half-height δ as the reference length, and the friction velocity u_τ as the reference velocity. These give rise to a reference Reynolds number $Re_\tau = u_\tau \delta/\nu$. As a first investigation of the proposed VMS formulation, we perform simulations at $Re_\tau = 180$. The centerline Mach number was set to $\mathrm{M} = 0.3$, so that the results can be directly compared [4,5,23] to the incompressible DNS data of Kim et al. [16]. The size of the computational domain is $(6\delta, 2\delta, 4\delta)$ in the x_1, x_2, and x_3-directions respectively. As shown by various investigations [13,22,29,30], these dimensions are sufficiently large for this Reynolds number. All simulations were started from an instantaneous incompressible DNS solution (obtained from an external code) projected onto the finite element basis under consideration. The time step (non-dimensionalized with u_τ and δ) was set equal to $\Delta t = 0.002$ for all simulations. This resulted in a maximum Courant number of approximately 0.2 for the mesh with the finest spatial resolution. Based on test computations over a range of time steps, with the current third-order accurate time discretization this value provides sufficient time resolution to allow the errors to be dominated by spatial resolution effects.

In the following, we compare results obtained using no SGS model to results obtained by applying the SGS model directly to all resolved scales, referred to as traditional LES, and results obtained from the VMS method, in which the direct effect of the SGS model is restricted to the small resolved scales. The Smagorinsky constant used in the traditional LES method is set to equal to $C_s = 0.1$, as this value has proven successful for turbulent channel flow in many prior numerical experiments. Additionally, van Driest damping is employed within the traditional LES method to account for the diminishing turbulent length scales as the solid walls are approached. As suggested by Hughes [11], the SGS model within the VMS method employs a modified value of the Smagorinsky constant used in the traditional model. This generally leads to higher values of C_s, as fewer modes must now produce an equivalent amount of dissipation compared to the traditional method. However,

we emphasize that no additional attempts were made to tune the Smagorinsky constant in order to improve the obtained results.

5.3. Coarse mesh results

We begin with $(8 \times 8 \times 8)$ elements with uniform polynomial degree $P = 2$. This resolution corresponds to element spacings of $\Delta x^+ = 135$ and $\Delta z^+ = 90$ in the streamwise and spanwise directions, and $\Delta y^+ \approx 14.6$ in the wall-normal direction. Note that since this is a high-order accurate method ($P > 1$), the cut-off wavenumber corresponds to $k_c = 8$.

Obviously, for polynomial degree $P = 2$, there is only one possibility for the VMS partition, that is $\widetilde{P} = 2$. This corresponds to the large scales being represented by just the linear modes in each direction (Section 3), while the small scales are the remaining modes having a quadratic variation in one or more of the coordinate directions. Fig. 5 shows the results obtained for the mean velocity profile (a), the rms profiles (b), the Reynolds stress (c), and the one-dimensional streamwise energy spectrum evaluated at $y^+ = 5.39$ (d). Overall, the results are in poor agreement with the DNS for all three methods. However, note that the Reynolds-stress obtained from the VMS method is closest to the DNS. Furthermore, the energy content in the first few modes of the energy spectrum obtained by the VMS method is closest to the DNS, while using no SGS model leads to excessive energy content throughout the entire wavenumber range. Applying the SGS model on all scales as in traditional LES methods, on the other hand, leads to results that suffer from excessive dissipation.

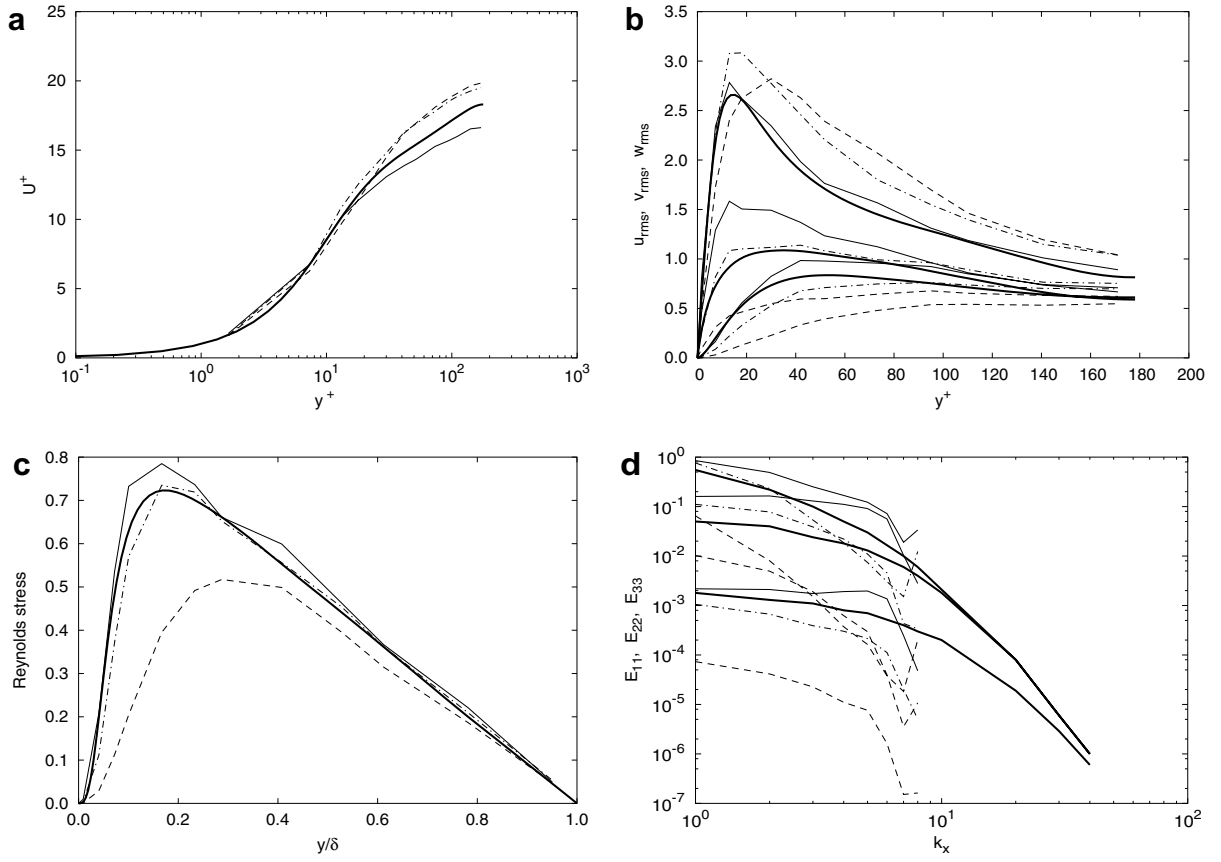

Fig. 5. Mean velocity (a); rms profiles (b); Reynolds stress (c) and one-dimensional streamwise energy spectrum ($k_c = 8$) (d) for $Re_\tau = 180$ obtained using $(8 \times 8 \times 8)$ elements with $P = 2$: —, DNS [16]; —, no model; ---, LES; –·–, VMS with $\widetilde{P} = 2$.

Clearly, the above resolution is too coarse for obtaining reasonable low-order statistics. Note that, in both the LES and VMS results, the basic dynamics of the important coherent structures, i.e. the near-wall streaks, are directly influenced by the SGS model. The spanwise element size ($\Delta z^+ = 90$) is approximately equal to the mean streak separation in spanwise direction. This means that the streamwise velocity profile in the spanwise direction varies from a high to a low and back to a high value again within one element, as sketched in Fig. 6. Note that such variation cannot be captured by the large-scale solution, which consists of only linear basis functions. The quadratic modes do have the capability of capturing such velocity variation within the element, however, these modes are contained within the small-scale space. Consequently, the SGS model is acting directly on those scales which describe the high to low velocity variation.

5.4. Uniform h-refinement

Next, we consider the effect of h-refinement in all spatial directions by employing ($16 \times 16 \times 16$) elements with $P = 2$. This mesh has a streamwise spacing of $\Delta x^+ = 67.5$, a spanwise spacing of $\Delta z^+ = 45$, and a wall-normal spacing of $\Delta y^+ \approx 5.9$. The cut-off wavenumber for this resolution corresponds to $k_c = 16$. Note that the spanwise element size now corresponds to half the typical streak spacing, or the streak size. As illustrated in the right graph of Fig. 6, the alternating spanwise velocity variation typical of near-wall streaks can now be captured by the linear modes on two neighboring elements. Since the linear modes are contained within the large-scale space, this feature of the near-wall streaks is not directly influenced by the SGS model.

The results for the mean velocity, rms profiles, Reynolds stress and one-dimensional streamwise energy spectrum are shown in Fig. 7a–d. The results obtained using no model are very similar to those at the coarse resolution, that is dominated by insufficient diffusive mechanisms. The mean velocity obtained using the model on all scales is in reasonable agreement with the DNS [16], while that obtained from the VMS method is indistinguishable from the DNS at this scale. Likewise, the best overall agreement with the DNS [16] of both rms profiles and Reynolds stress is obtained by the VMS method. It can be clearly seen from the energy spectrum that energy content obtained by the VMS method closely follows that of the DNS [16], while using the model on all scales again leads to excessive damping.

Fig. 8 shows an instantaneous contour-plot of the streamwise velocity in a horizontal plane in the near-wall vicinity of the flow, obtained from the VMS calculation. This figure clearly demonstrates that the near-wall streaks are captured, and confirms the typical streak spacings in streamwise ($\Delta x^+ \approx 400$) and spanwise direction ($\Delta z^+ \approx 100$).

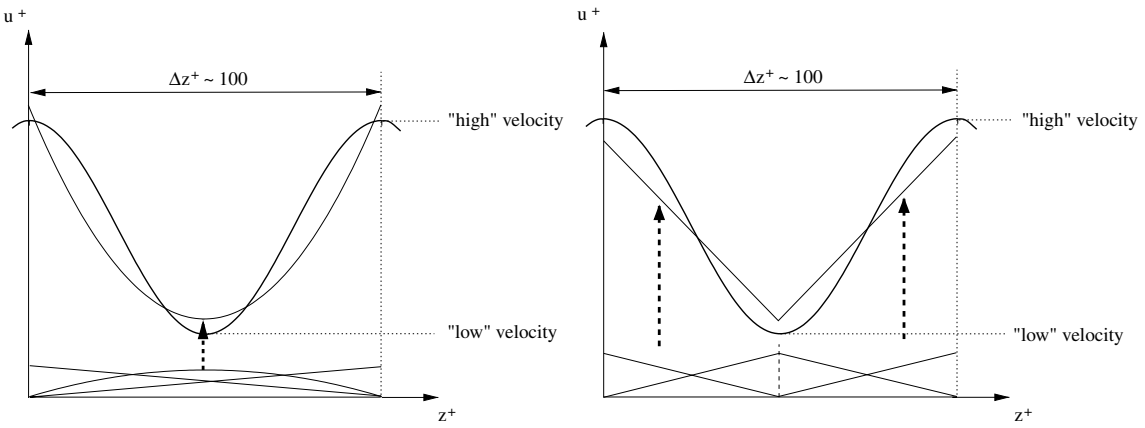

Fig. 6. Illustration of the near-wall streamwise velocity distribution in spanwise direction due to low-speed streaks, relatively to a spanwise element size. The modes at the bottom are the finite-element basis functions necessary to represent the velocity pattern associated with low-speed streaks for different number of elements in spanwise direction: 8 elements (left) and 16 elements (right).

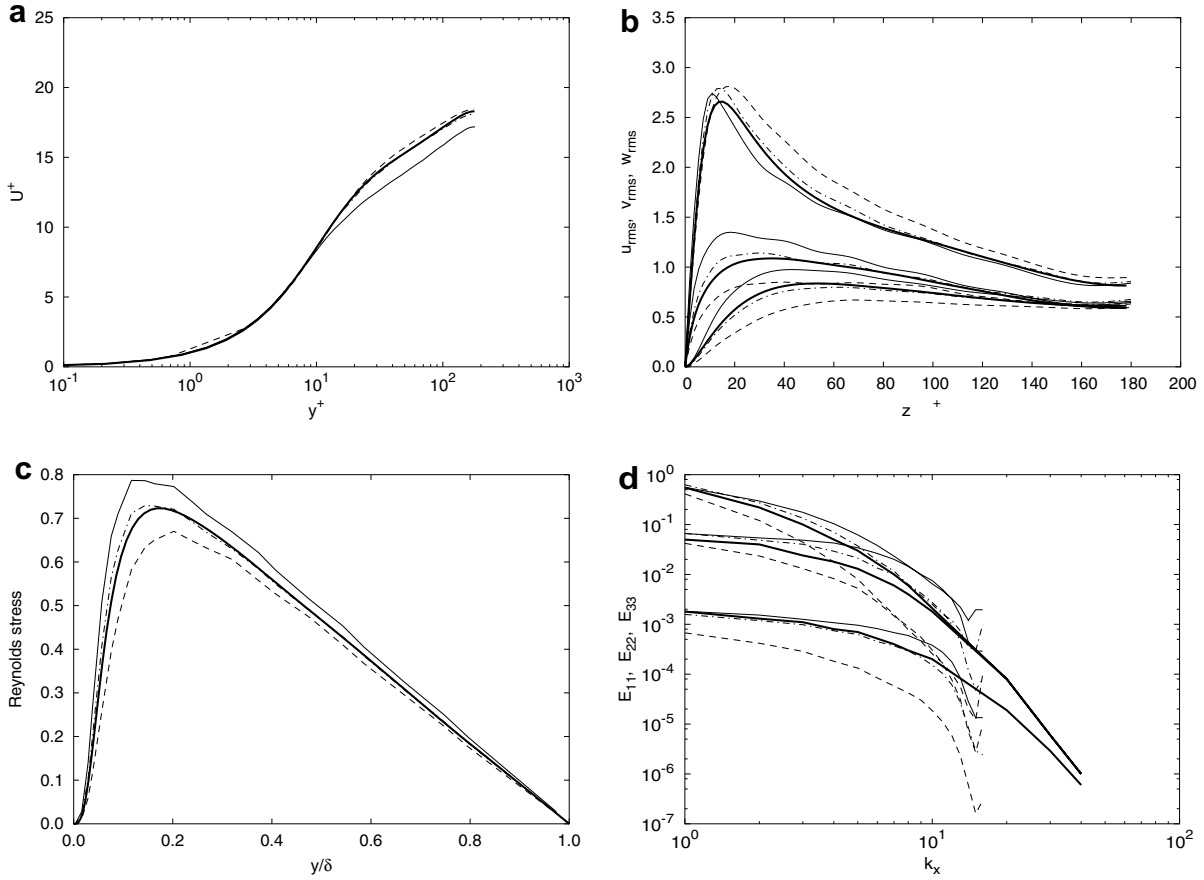

Fig. 7. Mean velocity (a), rms profiles (b), Reynolds stress (c), and one-dimensional streamwise energy spectrum ($k_c = 16$) (d) for $Re_\tau = 180$ obtained using $(16 \times 16 \times 16)$ elements with $P = 2$: —, DNS [16]; —, no model; ---, LES; – · – VMS with $\widetilde{P} = 2$.

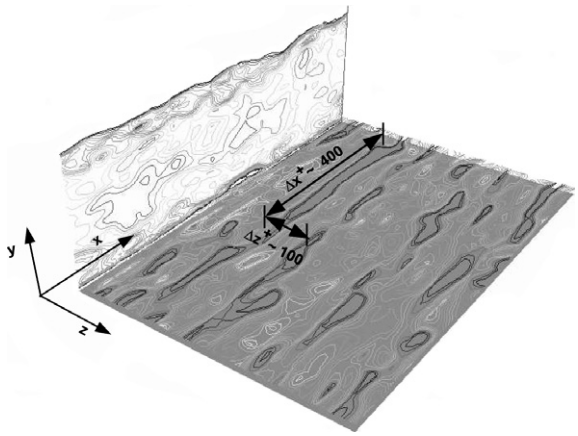

Fig. 8. Instantaneous streamwise velocity contours in a turbulent channel flow at $Re_\tau = 180$, obtained from a VMS calculation on $(16 \times 16 \times 16)$ elements with $P = 2$ and $\widetilde{P} = 2$.

5.5. Uniform p-refinement

Now, we investigate the effect of uniform p-refinement by employing $(8 \times 8 \times 8)$ elements with uniform polynomial degree $P = 3$. The cut-off wavenumber for this resolution corresponds to $k_c = 12$. Recall from Section 5.3 that the spanwise element size corresponds to the mean streak separation. Based on previous observations, we begin with a partition parameter $\widetilde{P} = 3$, so that the linear and quadratic modes are in the large scale space and all modes that contain a cubic term are considered small scales. This ensures that the quadratic modes, which are capable of capturing the basic streak velocity variation within an element (see Fig. 6), are not directly influenced by the SGS model.

As can be seen from Fig. 9, the best overall agreement with the DNS [16] is obtained using the VMS method. Both results obtained using no SGS model and those obtained by applying the SGS model to all scales are qualitatively very similar to the coarse resolution results of Section 5.3.

In order to further investigate the influence of the partition parameter on the results, we consider the effect of reducing the large-scale space by changing the large/small partition for the $(8 \times 8 \times 8)$ mesh to $\widetilde{P} = 2$. The modes containing quadratic and cubic terms are now contained within the small-scale space. Recall from our previous discussion that the quadratic modes, necessary to capture the streak velocity pattern within an element at this resolution, are then directly affected by the model. Fig. 10 compares the results obtained using the VMS method using $\widetilde{P} = 2$ to that of the VMS method with $\widetilde{P} = 3$ and the traditional LES method. Overall, the results of the VMS method with $\widetilde{P} = 2$ are in poor agreement with that of the DNS [16]. In fact, the results are of intermediate quality between the VMS method with $\widetilde{P} = 3$ and the LES method. These results again

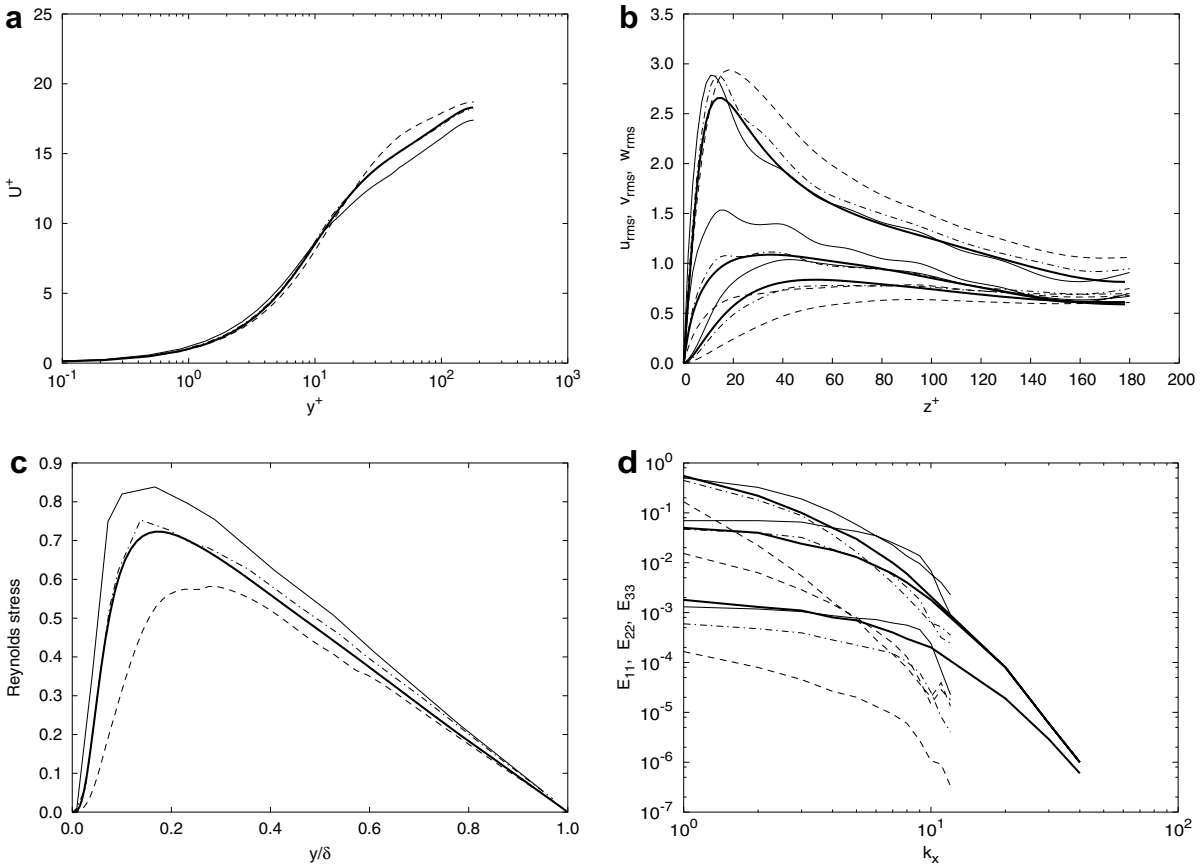

Fig. 9. Mean velocity (a), rms profiles (b), Reynolds stress (c), and one-dimensional streamwise energy spectrum ($k_c = 12$) (d) for $Re_\tau = 180$ obtained using $(8 \times 8 \times 8)$ elements with $P = 3$: —, DNS [16]; —, no model; ---, LES; – · –, VMS with $\widetilde{P} = 3$.

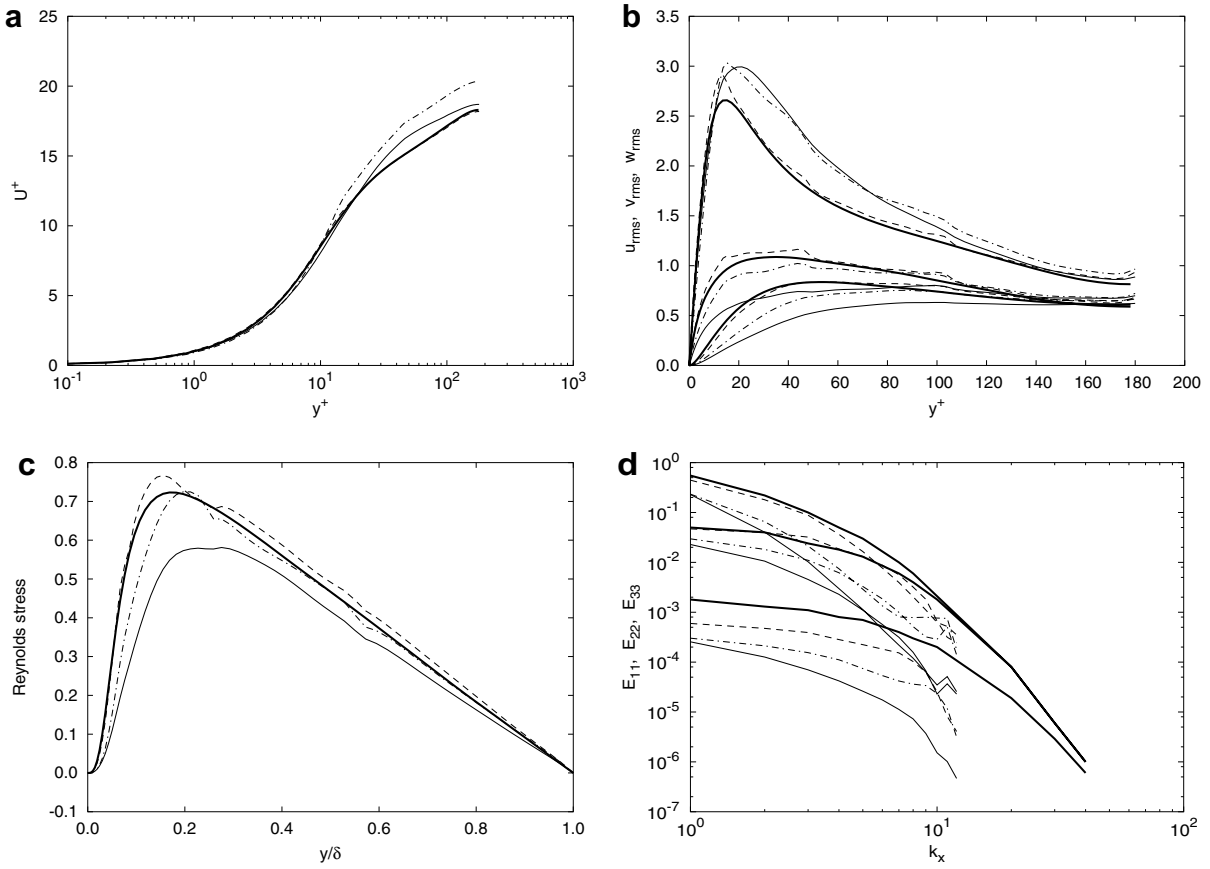

Fig. 10. Mean velocity (a), rms profiles (b), Reynolds stress (c) and one-dimensional streamwise energy spectrum (d) for $Re_\tau = 180$ obtained using $(8 \times 8 \times 8)$ elements with $P = 3$: — DNS [16]; —, LES; ---, VMS with $\widetilde{P} = 3$; – · –, VMS with $\widetilde{P} = 2$.

give a clear indication that modes representing the basic feature of the near-wall streaks should be left free from direct modeling terms.

6. Concluding remarks

We have considered the performance of a spatially-continuous modal-based VMS discretization for the simulation of fully-developed turbulent channel flows. The discretization was found to be capable of producing good low-order turbulent statistics at relatively coarse levels of refinement, provided that the fundamental modes of the largest near-wall coherent structures were contained within the model-free part of the basis. This indicates that in spite of the reduced orthogonality of the modal basis, its scale separation is sufficient to allow the present method to exploit the main advantages of the VMS approach.

The formulation of the method allows it to be applied to complex flow geometries while using relatively few degrees of freedom. This raises the issue of how the VMS approach is best applied when approaching a new flow. In the case that the scale of the most important structures is known a priori, then one can select the scale partition so that the fundamental modes of these structures can be represented in the model-free part of the solution basis. When approaching completely unknown flows, however, one must first resort to performing resolution studies in order to identify the most relevant phenomena for the quantity of interest. If a jump in accuracy is observed through variation of the partition parameter, however, correlations with physical flow features should be sought. The experienced gained can then be used to compute similar problems with minimal degrees of freedom, potentially exploiting locally-varying choices for the mesh size, P and $\widetilde{P}$. This appears to be a clear advantage of VMS-LES over single-scale approaches.

References

[1] S.S. Collis, Monitoring unresolved scales in multiscale turbulence modeling, Phys. Fluids 13 (2001) 1800–1806.
[2] S.S. Collis, The DG/VMS method for unified turbulence simulation, AIAA paper 2002-3124, 2002.
[3] S.S. Collis, Multiscale methods for turbulence simulation and control, in: 32nd Computational Fluid Dynamics Lecture Series, von Karman Institute, 2002.
[4] S.S. Collis, K. Ghayour, Discontinuous Galerkin methods for compressible DNS, in: Proceedings of FEDSM, ASME/JSME Joint Fluids Engineering Conference, 2003.
[5] S.S. Collis, S. Ramakrishnan, The local variational multiscale method, in: Third MIT Conference on Computational Fluid and Solid Dynamics, 2005.
[6] G. Hauke, T.J.R. Hughes, A comparative study of different sets of variables for solving compressible and incompressible flows, Comput. Methods Appl. Mech. Engrg. 153 (1998) 1–44.
[7] T.J.R. Hughes, Multiscale phenomena: Green's functions, the Dirichlet-to-Neumann formulation, subgrid scale models, bubbles and the origins of stabilized methods, Comput. Methods Appl. Mech. Engrg. 127 (1995) 387–401.
[8] T.J.R. Hughes, A space–time formulation for multiscale phenomena, J. Comp. Appl. Math. 74 (1996) 217–229.
[9] T.J.R. Hughes, V.M. Calo, G. Scovazzi, Variational and multiscale methods in turbulence, ICES report 04-46, 2004.
[10] T.J.R. Hughes, G.R. Feijóo, L. Mazzei, J.B. Quincy, The variational multiscale method – a paradigm for computational mechanics, Comput. Methods Appl. Mech. Engrg. 166 (1998) 3–24.
[11] T.J.R. Hughes, L. Mazzei, K.E. Jansen, Large eddy simulation and the variational multiscale method, Comp. Vis. Sci. 3 (2000) 47–59.
[12] T.J.R. Hughes, L. Mazzei, A.A. Oberai, The multiscale formulation of large eddy simulation: decay of homogeneous isotropic turbulence, Phys. Fluids 13 (2001) 505–512.
[13] T.J.R. Hughes, A.A. Oberai, L. Mazzei, Large eddy simulation of turbulent channel flow by the variational multiscale method, Phys. Fluids 13 (2001) 1784–1799.
[14] K.E. Jansen, A.E. Tejada-Martínez, An evaluation of the variational multiscale method for large-eddy simulation while using a hierarchical basis, AIAA paper 2002-0283, 2002.
[15] E.M. Karniadakis, S.J. Sherwin, Spectral/hp Element Methods for CFD, Oxford University Press, Oxford, 1999.
[16] J. Kim, P. Moin, R. Moser, Turbulence statistics in fully developed channel flow at low Reynolds number, J. Fluid Mech. 177 (1987) 133–166.
[17] B. Koobus, C. Farhat, A variational multiscale method for the large eddy simulation of compressible turbulent flows on unstructured meshes – application to vortex shedding, Comput. Methods Appl. Mech. Engrg. 193 (2004) 1367–1383.
[18] M.P. Martin, U. Piomelli, G.V. Candler, Subgrid-scale models for compressible large-eddy simulations, Theoret. Comput. Fluid Dynamics 13 (2000) 361–376.
[19] E.A. Munts, Space–time multiscale methods for large Eddy simulation, PhD thesis, Delft University of Technology, 2006.
[20] A.A. Oberai, T.J.R. Hughes, The variational multiscale formulation of LES: channel flow at $Re = 590$, AIAA paper 2002-1056, 2002.
[21] S.B. Pope, Turbulent Flows, Cambridge University Press, Oxford, 2000.
[22] S. Ramakrishnan, S.S. Collis, Partition selection in multiscale turbulence modeling, Phys. Fluids 8 (2006).
[23] S. Ramakrishnan, S.S. Collis, Multiscale modeling for turbulence simulation in complex geometries, AIAA paper 2004-0241, 2004.
[24] S. Ramakrishnan, S.S. Collis, Turbulence control using the variational multiscale method, AIAA J. 42 (2004) 745–753.
[25] S. Ramakrishnan, S.S. Collis, The local variational multi-scale method for turbulence simulation, Sandia Report, SAND2005-2733, 2005.
[26] H. Schlichting, K. Gersten, Boundary Layer Theory, eighth revised and enlarged ed., Springer, Berlin, 2000.
[27] F. Shakib, Finite element analysis of the compressible Euler and Navier–Stokes equations, PhD Thesis, Stanford University, 1988.
[28] J. Smagorinsky, General circulation experiments with the primitive equations. I. The basic experiment, Mon. Weather Rev. 91 (1963) 99–164.
[29] A.W. Vreman, The filtering analog of the variational multiscale method in large-eddy simulation, Phys. Fluids 15 (2003) L61–L64.
[30] W. Wang, Coupled compressible and incompressible finite volume formulations for the large eddy simulation of turbulent flow with and without heat transfer, PhD thesis, Iowa State University, 1995.